The South Indian Convergence Zone and Interannual Rainfall Variability over Southern Africa

KERRY H. COOK

Department of Earth and Atmospheric Sciences, Cornell University, Ithaca, New York

(Manuscript received 1 July 1999, in final form 9 December 1999)

ABSTRACT

The South Indian convergence zone (SICZ) is identified in this paper as a region of enhanced precipitation extending off the southeast coast of southern Africa during austral summer. Unlike the South Pacific convergence zone, the SICZ is a land-based convergence zone (LBCZ), with position and intensity at least partially determined by surface conditions over southern Africa. An idealized GCM simulation is used to explore the basic dynamics of LBCZs in the Tropics and subtropics. Output from a realistic GCM simulation and the National Centers for Environmental Prediction–National Center for Atmospheric Research 40-Year Reanalysis are analyzed to apply this basic dynamical framework to the case of the SICZ.

In contrast to the intertropical convergence zone where column moisture convergence is primarily due to meridional wind convergence in the moist environment, precipitation within the SICZ and the LBCZs in general is also supported by zonal wind convergence, moisture convergence by transient eddy activity, and moisture convergence associated with moisture advection. This fact suggests that interactions between transient and stationary eddy features and between tropical and midlatitude disturbances are key to understanding variability of the SICZ. In a GCM ensemble simulation of the response to ENSO-like warming in the eastern Pacific, the SICZ shifts northeastward because of a weakening of the western portion of the South Indian high. This shift results in the dipole precipitation pattern, with higher precipitation to the northeast and lower precipitation to the southwest, that is observed in connection with drying over southern Africa during warm events.

1. Introduction

Connections between the large-scale circulation and precipitation over southern Africa suggest the existence of a diagonally oriented convergence zone, the South Indian convergence zone (SICZ), off the southeast coast of southern Africa (Cook 1998). Considering the dynamics of the SICZ provides a way of ascribing physical mechanisms to some aspects of precipitation variability over southern Africa.

Figure 1a shows mean January precipitation for the Tropics, formed by averaging satellite-derived values from 1987 to 1998. These precipitation rates, the global precipitation index (GPI), are based on IR measurements using the algorithm described in Arkin and Meisner (1987). The South Pacific convergence zone (SPCZ) is clearly represented extending diagonally toward the southeast from the western Pacific warm pool. There is a weaker band of precipitation extending from the southeast coast of South America. This is the South Atlantic convergence zone (SACZ), which is not as well-known as the SPCZ but has received considerable attention in the literature for its role in determining South American precipitation distributions (e.g., Lenters and Cook 1995, 1999; Paegle and Mo 1997).

A similar structure in the precipitation field off the southeast coast of Africa is less distinct. A northwest–southeast orientation is present, but it separates less clearly from the intertropical convergence zone (ITCZ) than the SACZ and SPCZ and does not have a well-defined extension toward middle latitudes.

The SICZ may be more intermittent than the SACZ, and its presence is more apparent on certain shorter time averages. For example, the SICZ is clearly seen in the January 1994 mean precipitation (Fig. 1b); it is even more distinct than the SACZ. A survey of the austral summer seasons included in the GPI satellite precipitation climatology shows that the SICZ is well formed during about half of the austral summer season January and December averages (during 1988/89, 1991/92, 1992/93, 1993/94, and 1995/96).

This paper explores the basic hydrodynamics of land-based convergence zones (LBCZs) in the Tropics and subtropics and uses this framework to identify the SICZ as distinct from the ITCZ. The response of the southern African precipitation field to ENSO SST anomalies (SSTAs) in a model is examined, and a mechanism for

Corresponding author address: Dr. Kerry H. Cook, Dept. of Earth and Atmospheric Sciences, Cornell University, 3114 Snee Hall, Ithaca, NY 14853.
E-mail: khc6@cornell.edu

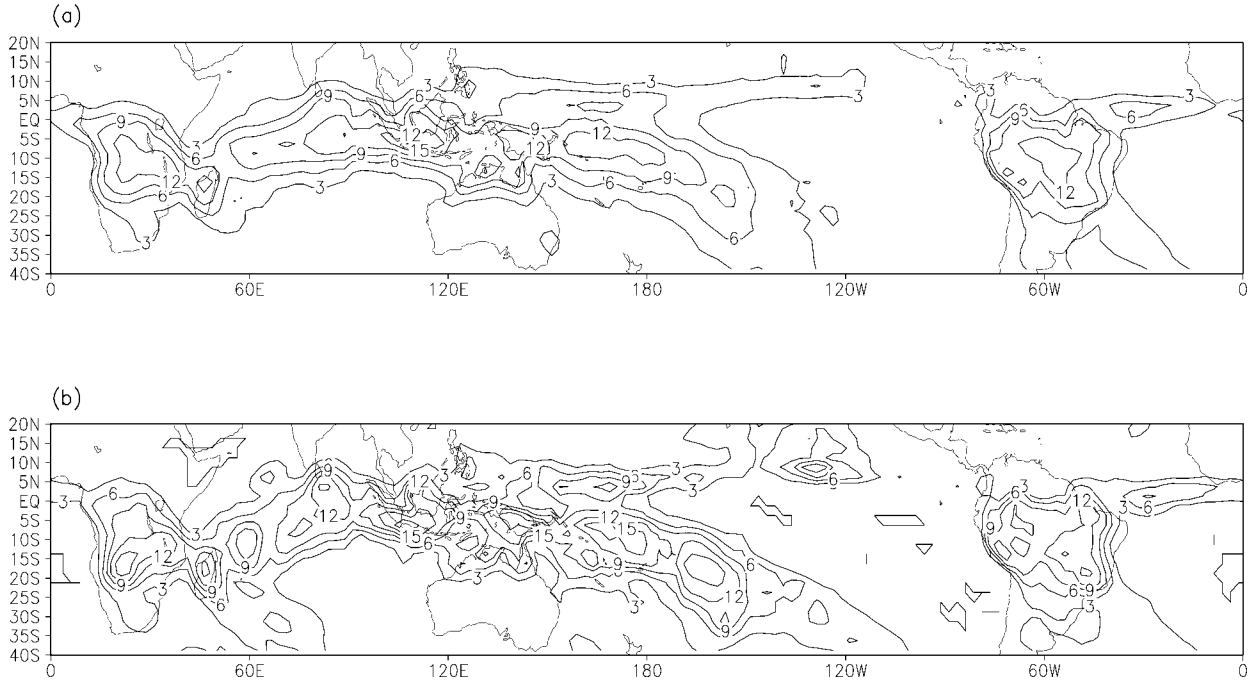

FIG. 1. Precipitation from GPI satellite-gauge observations for (a) the 1987–98 Jan average and (b) Jan 1994. Contour interval is 3 mm day^{-1}.

the occurrence of drought over parts of southern Africa during El Niño events is suggested.

A brief overview of some previous work on southern African precipitation and its variability is presented in the following section. Section 3 is a discussion of the fundamental dynamics of LBCZs using results from an idealized GCM simulation. In section 4, this framework is used to guide an examination of the SICZ in a realistic GCM simulation and in the National Centers for Environmental Prediction–National Center for Atmospheric Research (NCEP–NCAR) 40-Year Reanalysis. The role of the SICZ in determining southern Africa's response to ENSO is presented in section 5, and section 6 contains a summary and discussion of the results.

2. Background

A diagonal bond of strong precipitation extending off the continent to the southeast has long been noted as a feature of the mean climate of southern Africa. Some authors, such as Taljaard (1953) and Tyson (1986; Fig. 5.6), describe this region as a poleward excursion of the ITCZ to 15°S or more over southeastern Africa and an extension eastward over the subtropical Indian Ocean. Other studies, however, note similarities with the SACZ and SPCZ. For example, Streten (1973) identifies three preferred regions for slowly moving or semistationary cloud bands in the Southern Hemisphere, which are essentially the SPCZ, SACZ, and SICZ. Kuhnel (1989) and Lyons (1991) note a tropical upper-tropospheric trough off the southeast coast of Africa in summer, similar to the troughs that mark the SPCZ and the SACZ.

Southern African precipitation shows high variability on all timescales; see Mason and Jury (1997) for a comprehensive review. Some of this variability has been associated with the local ocean environment. The proximity of the Agulhas, Benguela, and Antarctic circumpolar currents leads to complex and highly variable SSTs around southern Africa (Shannon et al. 1990). Walker and Shillington (1990) and Mason (1995) show that this oceanic variability is expressed in the regional precipitation field on intraseasonal to interannual timescales. Nicholson and Entekhabi (1987) examine the relationship between SSTAs in the Benguela upwelling region and precipitation over southern Africa. They suggest that the high correlations do not represent a causal relationship but that the SSTs and precipitation are both responding to atmospheric forcing over the South Atlantic.

Several studies reveal a dipole pattern in precipitation, convective activity, and outgoing longwave radiation (OLR) variability over southern Africa during the summer. The dipole represents an anticorrelation between eastern Africa south of about 20° latitude and locations to the northeast, including much of Madagascar. The dipole pattern arises on all timescales, from daily (Todd and Washington 1998; Lyons 1991) to interannual (e.g., Lindesay 1988; Jury 1992). In the paper, the dipole pattern is interpreted as movement of the SICZ.

Southern African precipitation emerges as sensitive to ENSO SSTAs in many observational studies that correlate precipitation with the Southern Oscillation index (SOI; e.g., Stoeckenius 1981; Ropelewski and Halpert 1987; Janowiak 1988). Lindesay (1988) finds that stronger correlations exist later in the summer rainy season (January–March) and associates about 20% of the rainfall variance with the SOI.

There are two possible pathways for communicating the ENSO signal into the southern African precipitation field. One is contained wholly within the atmosphere. A purely atmospheric mechanism, which is related to Rossby wave generation that results from an adjustment of the equatorial Walker circulation to ENSO SSTAs, is identified by Cook (2000, manuscript submitted to *J. Atmos. Sci.*, hereinafter C00) in ensemble GCM simulations (see section 5). The second pathway involves interactions between the atmosphere and oceans. For example, if the atmosphere responds to east Pacific SSTAs in a way that causes warming in the Indian Ocean [as in Latif and Barnett's (1995) modeling study], the southern African precipitation field may respond through a sensitivity to these more local SSTAs (e.g., Nicholson and Kim 1997).

Despite the statistical correlation between rainfall and SOI, not every ENSO year is dry over South Africa. A prime example is the strong warm event of 1997/98. While southern Zimbabwe and Namibia experienced drought during this summer, most of southern Africa had normal precipitation amounts for the season despite a dry start to the summer rainy season. [See the Web site for the African desk maintained the National Oceanic and Atmospheric Administration (NOAA) Center for Climate Prediction (CPC): http://www.cpc.ncep.noaa.gov/products/african_desk/] Some observational studies suggest that the ENSO signal is not very strong in southern Africa and that interannual variability in southern African precipitation is largely a response to Indian and/or southern Atlantic Ocean SSTAs that may not be causally connected to the ENSO cycle (e.g., Mason 1995; Nicholson and Kim 1997). Other studies suggest a prominent role for the quasi-biennial oscillation (QBO) phase in influencing summer precipitation through modification of the Walker circulation (e.g., Jury et al. 1994).

3. Fundamental hydrodynamics of the SICZ: Theoretical framework

The formation of a convergence zone is part of the basic response of the summer hemisphere atmosphere to the presence of land in the Tropics and subtropics. Cook (1994) diagnoses precipitation perturbations associated with a featureless land surface in the Tropics in a low resolution atmospheric GCM and explores changes in the precipitation perturbation due to prescribed changes in soil moisture. Regardless of how dry the land surface becomes, precipitation is enhanced over the eastern portion of the land surface and in a diagonal strip that extends poleward and to the east of the land surface [Fig. 2 in Cook (1994)].

A similar GCM is used here to investigate LBCZs in their most rudimentary form. The GCM is a version of the Geophysical Fluid Dynamics Laboratory (GFDL) GCM with simple physics, including moist convective adjustment, prescribed cloud fraction, perpetual austral summer insolation, and surface bucket hydrology. A single, flat block continent is specified at the surface, with prescribed, zonally uniform SSTs. Land and sea surface albedo is a uniform 0.1, surface roughness over land is greater than over the ocean to stimulate a deeper mixed layer, and soil moisture is prescribed at 5 cm everywhere. The simulation is identical to one discussed in Cook (1994) except a higher resolution (R30) is used and the SSTs are more representative, being the zonal mean of the Shea et al. (1992) climatology. The continental outline, prescribed SSTs, and land surface temperatures averaged over a 1500-day integration are depicted in Fig. 2.

Figure 3a shows the precipitation distribution from the model climatology. The strength of the ITCZ is reasonable, with its axis near the equator over the broad, flat SST maximum (Fig. 2). The precipitation field over land has the shape of a ''Y'' lying on its side; this structure is seen in the observations when the SICZ is well defined (Fig. 1b). There are two maxima, one in the east and one in the west. [Cook (1997) discusses how similar maxima are maintained in relation to the land surface conditions over northern Africa in boreal summer.] A zone of enhanced precipitation stretches diagonally off the east coast in the summer hemisphere; this is an LBCZ analogous to the SICZ and the SACZ.

A first-order understanding of this precipitation distribution comes from considering the relative importance of evaporation and vertically integrated moisture convergence:

$$\overline{P} = \overline{E} - \overline{\int_0^{p_s} \nabla \cdot (q\mathbf{v}) \frac{dp}{g\rho_w}}, \tag{1}$$

where P is precipitation rate, E is evaporation rate, p_s is surface pressure, q is water vapor mixing ratio, $\mathbf{v}$ is the three-dimensional wind vector, ρ_w is the density of water, and the overbars indicate a time period that is long enough so that $\overline{(\partial q/\partial t)}_p \approx 0$. Evaporation rates are comparable in magnitude to the precipitation rates, but they do not mirror the structure seen in the precipitation field over the uniformly moist block continent. The ''Y'' structure in the precipitation field is apparent in the moisture convergence, so this term is further decomposed.

The time–mean vertically integrated moisture convergence within an atmospheric column, $\overline{Q}$, can be written as the sum of the convergence term ($\overline{C}$), orographic term ($\overline{O}$), advection term ($\overline{A}$), and transients term ($\overline{T}$):

$$\overline{Q} = \overline{C} + \overline{O} + \overline{A} + \overline{T}. \tag{2}$$

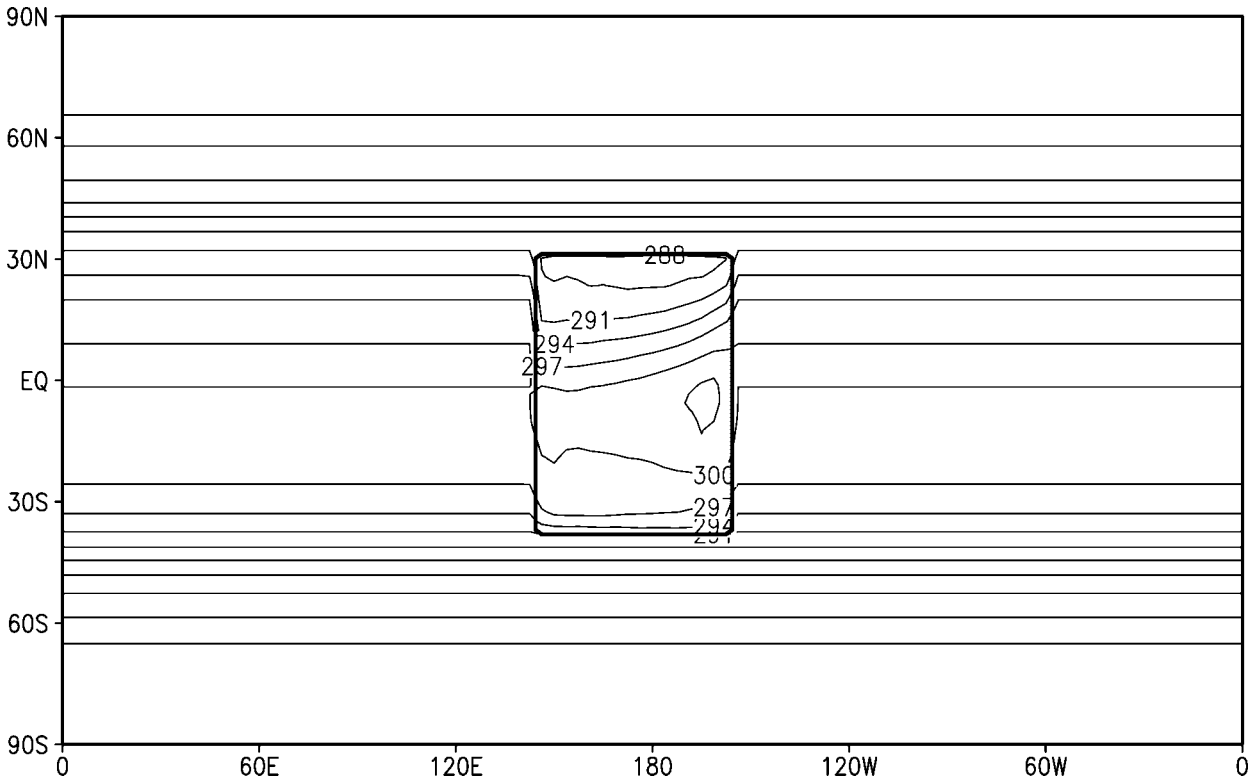

FIG. 2. Surface temperatures from the GCM simulation with a block continent with uniform soil moisture prescribed at 5 cm. Contour interval is 3 K.

Writing each component as an integral over $\sigma \equiv p/p_s$, the GCM's vertical coordinate, gives

$$\overline{C} = -\frac{\overline{p}_s}{g\rho_w}\int_0^1 \overline{q}(\boldsymbol{\nabla}_h \cdot \overline{\mathbf{v}})\, d\sigma, \tag{3}$$

$$\overline{O} = -\frac{1}{g\rho_w}\overline{(q\omega)}_s, \tag{4}$$

$$\overline{A} = -\frac{\overline{p}_s}{g\rho_w}\int_0^1 (\overline{\mathbf{v}} \cdot \boldsymbol{\nabla}_h \overline{q})\, d\sigma, \quad \text{and} \tag{5}$$

$$\overline{T} \approx -\frac{1}{g\rho_w}\boldsymbol{\nabla}_h \cdot \left[\int_0^1 (\overline{p_s q \mathbf{v}} - \overline{p}_s \overline{q}\,\overline{\mathbf{v}})\, d\sigma\right]. \tag{6}$$

[See Lenters and Cook (1995) for details of the derivation and the exact form of $\overline{T}$.]

Figures 3b,c,d show $\overline{C}$, $\overline{A}$, and $\overline{T}$ from the idealized GCM climatology; the orographic term is negligible for the flat continent. The term $\overline{C}$ reflects much of the structure of the precipitation field (Fig. 3b) over both the land and ocean. The LBCZ is strengthened and extended by the advection term (Fig. 3c), with enhanced precipitation persisting even 40°–50° longitude east of the land surface. The LBCZ is also a region in which transient water vapor fluxes play an important role in converging moisture. As seen in Fig. 3d, the transients weaken the precipitation maximum near 20°S and 170°W and act to shift the oceanic precipitation maximum toward the south or southwest. The contribution from transient activity may represent the effects of interactions with midlatitude waves, as seen in Lyons's (1991) study.

A decomposition of the convergence term (Fig. 3b) into its zonal and meridional components is shown in Fig. 4. Convergence over the eastern part of the continent in the summer hemisphere is primarily due to zonal convergence (Fig. 4a). Meridional convergence (Fig. 4b) is also influential, however, and shifts the convergence maximum southward. The ITCZ, the western continental precipitation maximum, and the southeastward extension over the ocean are supported primarily by meridional convergence; the latter two are weakened by zonal divergence.

Figure 5a shows the 866-mb flow and geopotential near the block continent. This level is representative of the troposphere below about 700 mb, where nearly all of the moisture convergence occurs. The heat low forms over the land surface between about 10° and 25°S. As is seen in observations, the subtropical highs over the oceans are centered 10°–15° latitude farther south compared with the heat low. The trough is placed off the southeast coast where the midlatitude isoheights dip equatorward.

The zonal convergence maximum near 5°S and 165°W (Fig. 4a) occurs where the flow in the northwest

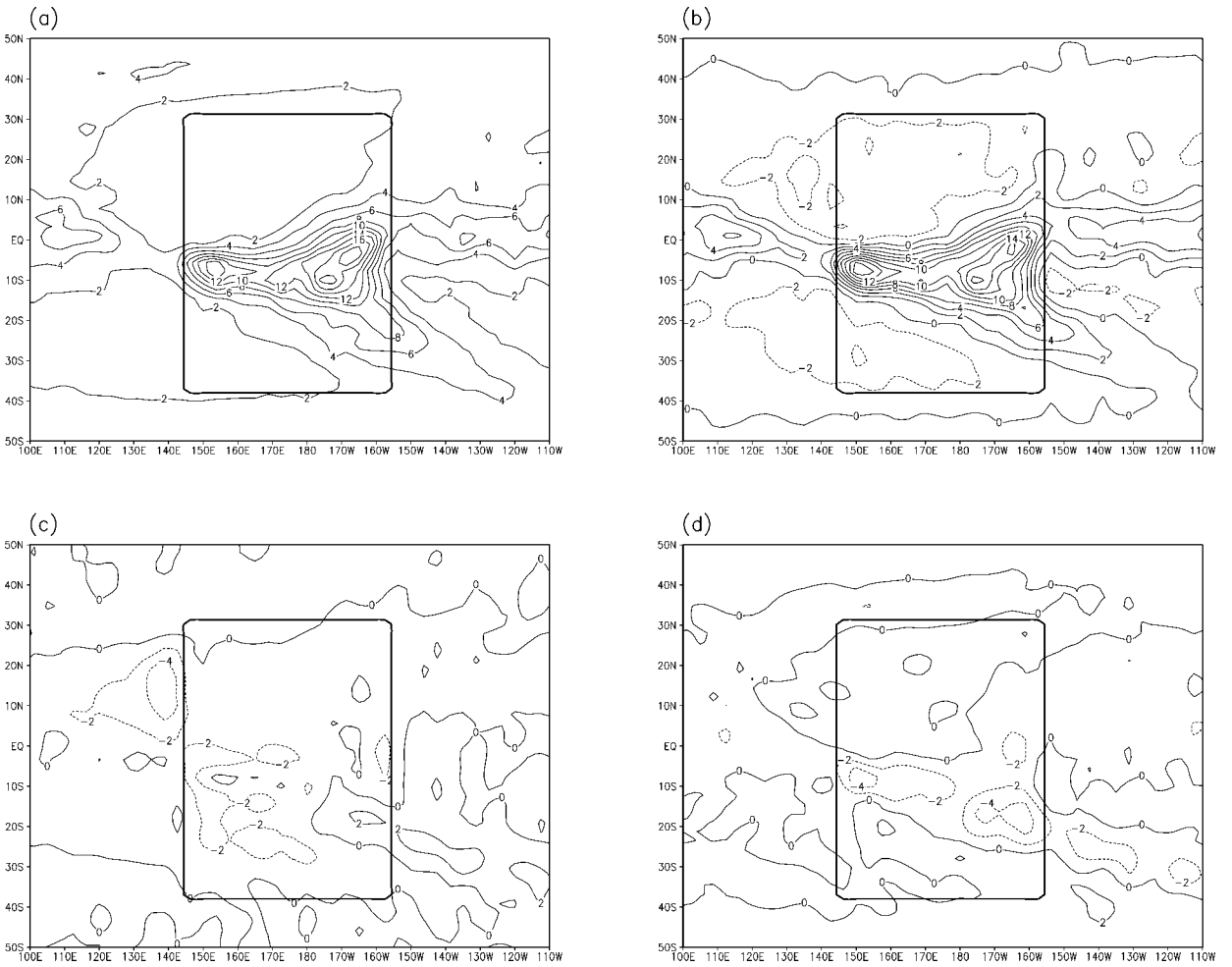

FIG. 3. (a) Precipitation, (b) convergence term [Eq. (3)], (c) advection term [Eq. (5)], and (d) transients term [Eq. (6)] from the idealized R30 GCM climatology. Contour interval is 2 mm day^{-1}.

quadrant of the subtropical high to the east of the land surface converges with flow in the northeast quadrant of the heat low. The cyclonic flow is a diversion of the strong winter hemisphere trades across the equator. Meridional divergence occurs at the same location as both flows turn southward. We refer to the region of strong zonal convergence as the ''root'' of the LBCZ and note that its formation is fundamentally different from that of the ITCZ.

Near 15°S and 160°W, the flow about the eastern subtropical high parallels the flow around the heat low (Fig. 5a). Meridional convergence results to the south as the northerly flow turns westward over the land and eastward over the ocean (Fig. 4b). Some of the meridional convergence is, therefore, balanced by zonal divergence (Fig. 4a). However, there is net horizontal convergence (Fig. 3b) where the southward flow out of the Tropics meets the northward component of the flow in the midlatitude trough. This meridional convergence supports the diagonal extension of the convergence zone over the ocean to the southeast. This region of meridional convergence is physically separate from the meridional convergence of the ITCZ by a region of meridional divergence.

Figure 5b shows the 866-mb flow with contours of water vapor mixing ratio. The flow in the southwest quadrant of the eastern subtropical high is nearly perpendicular to the moisture gradient. The low-level flow leaves the root zone of the LBCZ and advects moisture to the southeast, contributing to the diagonal extension of the convergence zone out over the ocean (Fig. 3c). There is no such contribution to moisture convergence within the ITCZ.

The LBCZ forms off the east coast, but not off the west coast, of the idealized continent in the GCM. There are two reasons for this asymmetry. One is that while there is low-level convergence over the western portion of the land surface analogous to the root zone of the LBCZ, there is no opportunity for strong moisture advection to occur off the coast given that the flow about the high is directed onshore and up the moisture gradient.

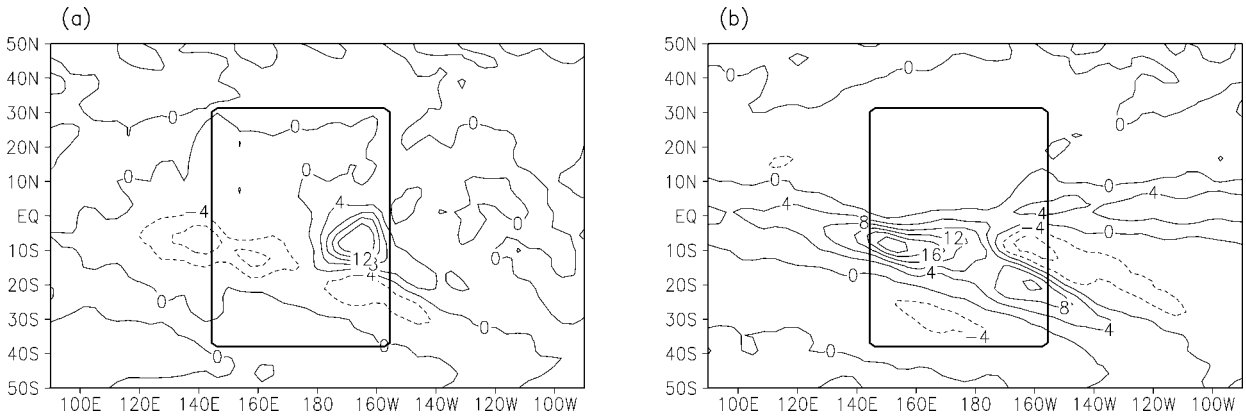

FIG. 4. Contours of the (a) zonal and (b) meridional components of the moisture convergence term at 866 mb in the idealized GCM simulation. Contour interval is 4 mm day^{-1}.

Considering the thermodynamic balance provides a second reason why the east is favored for LBCZ formation. In the summer hemisphere, isotherms dip poleward and geopotential heights dip equatorward over land surfaces. This results in warm air advection by the geostrophic wind in the east, which is balanced by the advection of lower potential temperature from lower levels. The resulting ascent may provide a trigger for the formation of LBCZs in the spring. Over the western portion of a continent, isotherms and isoheights are aligned in such a way that cold air advection and sinking result. A quantitative evaluation of this mechanism for the SICZ is provided below.

4. More realistic cases

a. GCM with realistic boundary conditions

The GCM with idealized boundary conditions was used to provide a simple framework for understanding why LBCZs form, but it may be a weak component of the full system. A GCM simulation with realistic boundary conditions and the NCEP–NCAR 40-Year Reanalysis are examined to provide more realistic cases.

The realistic GCM simulation is a 20-yr integration. Solar insolation, SSTs, soil moisture, cloud fraction, and land surface albedo are prescribed and change seasonally according to observations but are the same for each of the 20 yrs. SSTs are from the Shea et al. (1992) climatology, soil moisture is from Mintz and Walker (1993), and land surface albedo distributions are from Matthews (1983). Full continental outlines, including topography, are included.

Figure 6 shows the moisture budget components near southern Africa from the realistic GCM January climatology; shading in Figs. 6c–f indicate negative values. There is more structure in the continental precipitation field (Fig. 6a) as compared with the idealized case (Fig. 3a), but the basic large-scale ''sideways Y'' shape of the field is preserved, including an LBCZ extending to the southeast (the SICZ). A ''root zone'' is not prominent in the zonal wind convergence field (not shown), perhaps because of the presence of Madagascar and the Drakensburg Mountains along the east coast. Compared with observations (Fig. 1), the GCM produces too much rainfall over southeastern Africa and not enough over Madagascar. Also, the precipitation maximum over the interior is located about 5° latitude too far north. However, there is general agreement with the observations in the magnitude of the rainfall rates and the shape of the precipitation perturbation over the continent and within the ITCZ. Given the uncertainties in observing precipitation, the GCM is reproducing a reasonable precipitation field.

Unlike the idealized GCM case with uniform soil moisture, evaporation (Fig. 6b) plays a role in establishing the longitudinal gradient of precipitation across southern Africa in the summer hemisphere and the meridional gradient across the Sahel in the winter hemisphere. It also contributes to the SICZ hydrodynamics. Evaporation rates off the east coast of southern Africa are about twice those off the west coast, and these higher evaporation rates strengthen the SICZ. This is one way in which the presence of the warm Agulhas current of the western Indian Ocean can influence the SICZ.

As in the idealized case, much of the structure in precipitation over the land surface and within the ITCZ is associated with wind convergence (Fig. 6c). The advection (Fig. 6d) and transients (Fig. 6e) terms play significant roles within the SICZ, with the advection term extending the SICZ out over the ocean to the east and the transients shifting the SICZ to the southwest. The same effects occur in the idealized LBCZ (ref. Fig. 3).

The orographic term (Eq. 4) from the realistic GCM simulation contributes to the column moisture convergence in the expected regions, where the low-level flow impinges on topography. This contribution, shown in Fig. 6f, is estimated by linearly extrapolating the vertical moisture transport at the lowest model level to the surface. In the subtropics, low-level horizontal conver-

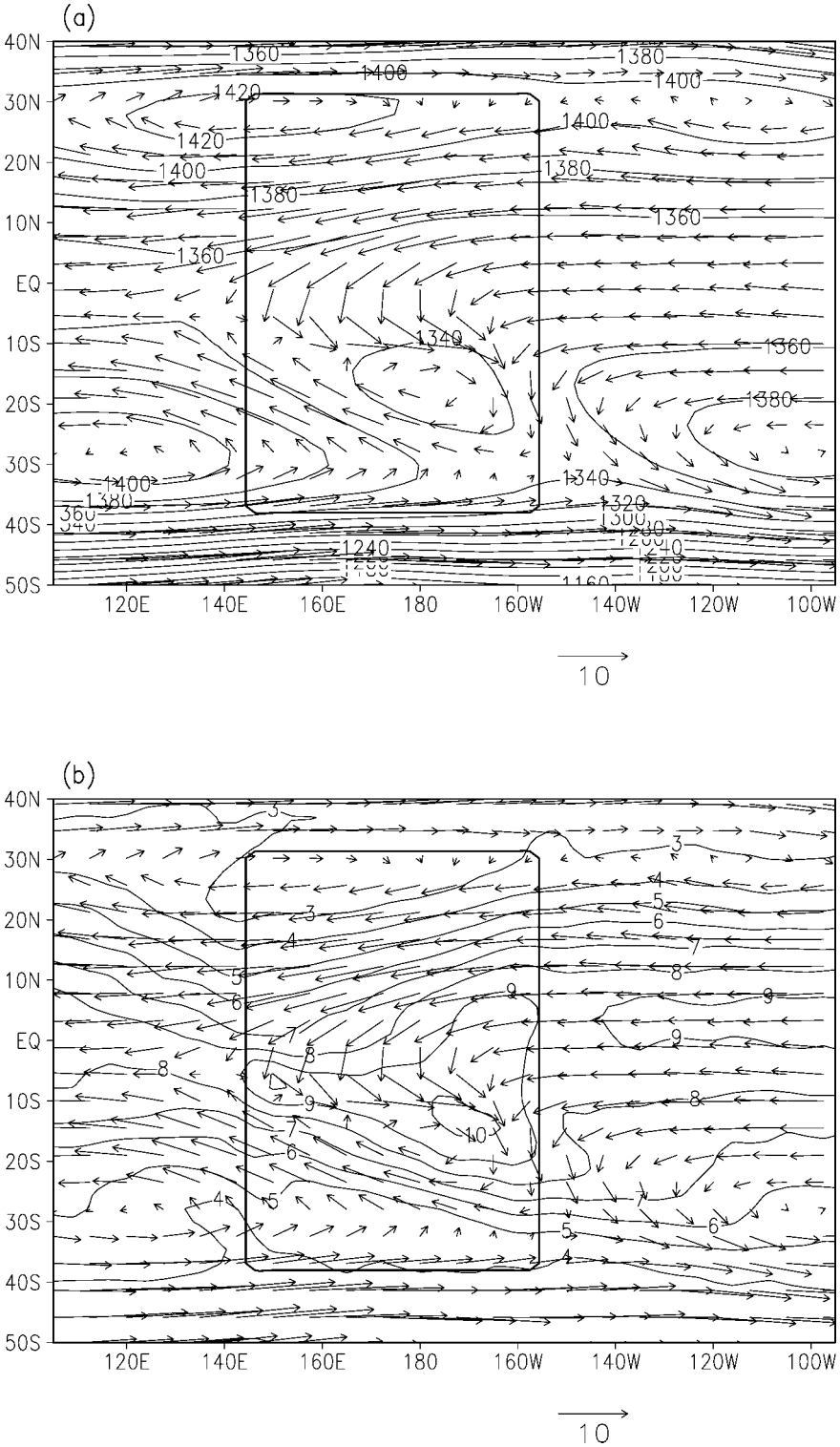

FIG. 5. (a) Geopotential height using 20-gpm contour intervals and (b) water vapor mixing ratio with 1 g kg^{-1} contour intervals at 866 mb from the idealized GCM climatology. Wind vectors are also included in each plot, and a wind scale (m s^{-1}) is indicated.

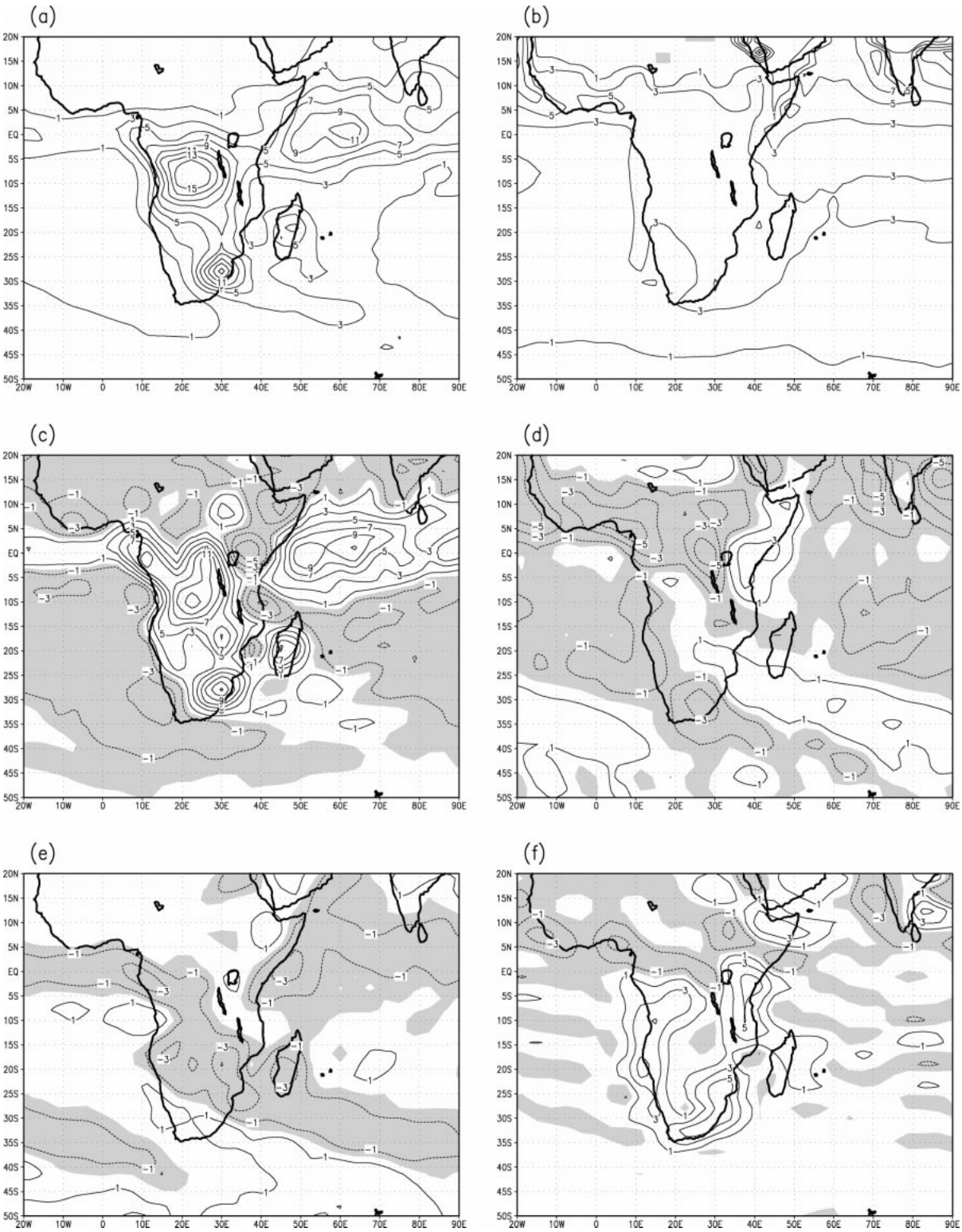

FIG. 6. (a) Precipitation, (b) evaporation, (c) convergence term [Eq. (3)], (d) advection term [Eq. (5)] (e) transients terms [Eq. (6)], and (f) orographic term [Eq. (4)] for the realistic GCM climatology. Contour intervals are 2 mm day^{-1}, and shading indicates negative values.

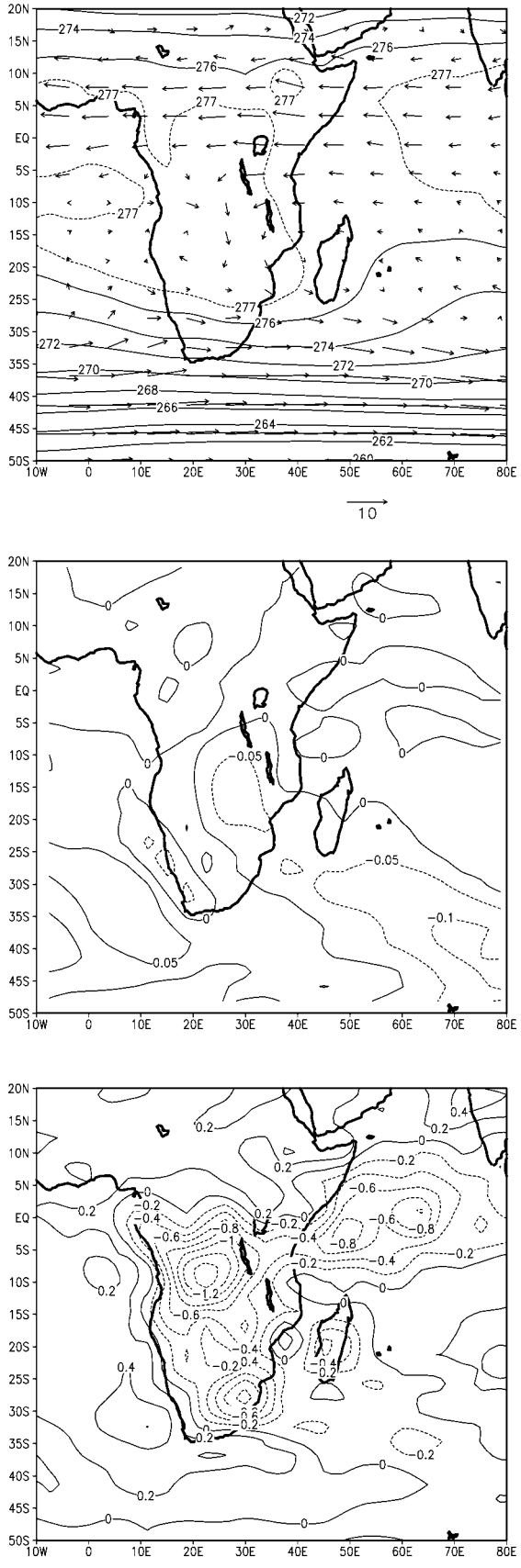

gence forced by condensational heating aloft tends to work in concert with mechanically forced vertical motion at the lower boundary to produce the net topographic influence (Ringler and Cook 1995). Contributions from both the orographic and convergence terms should be seen as the full topographic contribution. Both terms are important over Madagascar and the Drakensburg Mountains and may mask the zonal convergence that maintains the root zone in the idealized case (Fig. 4a). The orographic term is small over Madagascar, suggesting that the topography may not be resolved well enough in the R30 GCM to reproduce observed precipitation rates in that region. Over the southern tip of the continent, advection decreases precipitation. The overly strong moisture convergence on the southeast coast may also be related to the unrealistically low surface elevations that occur in GCMs, since a realistic wind convergence field will produce moisture convergence that is too strong if the moisture content of the air is too high.

As discussed in section 3, warm air advection in summer over the eastern portion of South America can provide a mechanism for generating vertical velocity and setting up the SACZ. The steady-state thermodynamic equation is

$$\mathbf{v}_h \cdot \nabla T - S\omega = \frac{Q}{c_p}, \tag{7}$$

where $S = -T(\partial \ln\theta/\partial p)$ and θ is potential temperature. Writing $\omega = \omega_A + \omega_Q$, where

$$\omega_A = \frac{1}{S}(\mathbf{v}_h \cdot \nabla T) \quad \text{and} \tag{8}$$

$$\omega_Q = -\frac{1}{S}\left(\frac{Q}{c_p}\right), \tag{9}$$

allows us to distinguish vertical motion induced by the horizontal flow (ω_A) from vertical motion induced by diabatic heating (ω_Q).

In the summer over southern Africa, geopotential heights are perturbed equatorward over the land surface, and isotherms are perturbed poleward. East of Africa, isotherms shift equatorward over the Indian Ocean. This structure is a consequence of the surface heat budget over the low–heat capacity land and the high–heat capacity water and is also related to the ocean surface currents.

Figure 7a shows isotherms and flow vectors, which are essentially geostrophic south of about 10°S, at 700 mb for December from the realistic GCM simulation.

←

FIG. 7. (a) 700-mb wind vectors and isotherms for Dec of the realistic GCM climatology. Contour interval is 2 K, with the 273-K isotherm dashed in. Wind vector scale: m s^{-1}. (b) Values of ω_A, with 0.05 Pa s^{-1} contour interval, and (c) ω_Q, with 0.2 Pa s^{-1} contour interval, from the realistic GCM simulation.

Cold air advection occurs just west of the continent from 0° to 20°E, and warm air advection occurs over the eastern part of the land surface and over the ocean to the east. The poleward excursion of the isotherms leads to additional warm air advection over the Indian Ocean southeast of Madagascar, even though the flow is not perturbed. As seen in Fig. 7b, which is a plot of ω_A, ascent is induced by this warm air advection over a region that is shaped very much like the SICZ. It is not obvious from a visual examination of the flow and isotherms in Fig. 7a, but another region of negative ω_A (ascent) is generated when the flow vectors turn slightly poleward when meeting the topography of southwestern South Africa. The descent associated with cold air advection is to the southwest of this feature.

Vertical velocities associated with diabatic heating are larger than vertical velocities associated with horizontal temperature advection. Figure 7c shows ω_Q from the GCM Dec climatology, and the pattern of the field closely resembles the precipitation, as would be expected. Magnitudes of ω_Q are up to an order of magnitude larger than those of ω_A, but the structure of the two fields is very different. Near the SICZ, the magnitude of ω_A is comparable to that of ω_Q.

b. NCEP–NCAR 40-Year Reanalysis

The realistic GCM analysis suggests that the LBCZ dynamics identified using the idealized case is applicable to understanding more realistic cases. To continue an exploration of the SICZ in realistic settings, the NCEP–NCAR 40-Year Reanalysis is examined. Components of the budget for the December climatology in the NCEP–NCAR 40-Year Reanalysis (1949–98; Kalnay et al. 1996), interpolated onto the GCM's R30 transform grid, are presented in Fig. 8. Precipitation rates (Fig. 8a) are about half of the satellite observed (Fig. 1) and modeled with the GCM (Fig. 6a), but the three maxima (central, Madagascar, and south) are captured. There is not a well-defined SICZ.

Evaporation rates are similar in the GCM and the reanalysis (Fig. 6b and 8b), since they derive primarily from soil moisture specifications. Precipitation over the oceans, the western and central parts of the continent, and Madagascar is supported by the convergence term in the reanalysis (Fig. 8c). This corresponds with the GCM results as well. The most prominent difference between the GCM and reanalysis convergence terms is on the east coast. Here, the reanalysis simulates strong column moisture divergence along the length of the east coast, while the GCM has only weak, isolated centers of moisture. These differences may be associated with orography (see below).

The importance of the moisture advection and transients terms off the southeast coast is represented in the reanalysis. The diagonal band of high moisture advection off the southeast coast in the reanalysis (Fig. 8d) is similar in magnitude and position to the corresponding structure in the GCM (Fig. 6d). The transients term (Fig. 8e) in the reanalysis is also very similar to that in the GCM.

Figure 8f shows an estimate of the orographic precipitation from the reanalysis. This term was calculated by extrapolating wind and moisture values to the surface using the two lowest pressure levels that are not underground.

The residual of the moisture budget terms shown in Fig. 8 is not small. Residual values as large as the precipitation rates shown in Fig. 8a are associated with the Ethiopian Plateau and the southeast coast mountains, suggesting that the orographic term (and maybe the convergence term) is in error. Computing the moisture budget on sigma surfaces, which are not available for the NCEP climatology, would improve the estimate of the moisture budget components.

This decomposition of the NCEP moisture budget suggests that the hydrodynamics of the LBCZ identified in the idealized GCM is realized in the reanalysis. In the following section, an application to understanding mechanisms of precipitation variability is presented. In particular, a mechanism to explain low precipitation rates over southern Africa during ENSO is suggested.

5. Precipitation variability

Because LBCZs are interfaces between continental thermal lows and oceanic subtropical highs, the intensity and position of an LBCZ will vary with changes in these features. For example, precipitation within the LBCZ will change with the intensity or position of the continental thermal low, perhaps due to changes in or feedbacks with surface conditions. Global-scale influences can propagate into the system by modifications of the subtropical high's shape, position, or magnitude. These connections provide a way of ascribing physical mechanisms to precipitation variability.

An example of using the concept of the SICZ to identify mechanisms of precipitation variability is presented by considering the response of the southern African precipitation field to a warm ENSO event in a GCM. As in the realistic GCM climatology discussed above, which is used as a control for the ENSO simulations, the ENSO integrations employ R30 resolution and 14 vertical levels on sigma surfaces. Base SSTs, surface albedos, and soil moisture are set to the same realistic and seasonally varying values.

The ENSO simulations use simplified but time-dependent SSTAs and address ENSO forcing in the context of seasonality and internal atmospheric variability. The ENSO SSTAs represent warming in the eastern Pacific only, with shape, timing, and magnitude based on observed warm ENSO events. The SST anomaly mimics a relatively mild event. It is Gaussian in shape, reaches a maximum of 2 K in November of the first year, and decays through the spring of the second year. C00 provides a more complete description of the choice

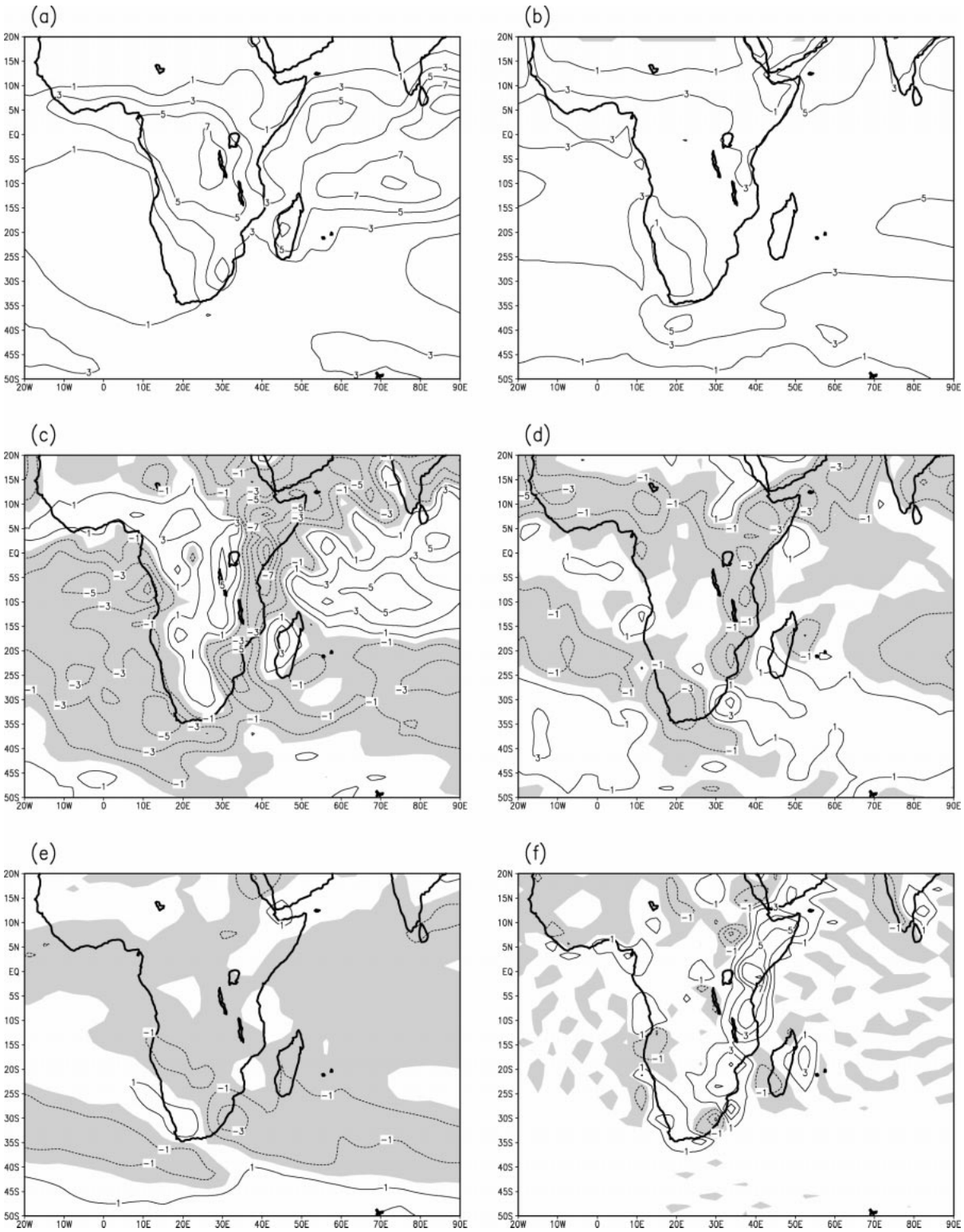

FIG. 8. (a) Precipitation, (b) evaporation, (c) convergence term [Eq. (3)], (d) advection term [Eq. (5)], (e) transients terms [Eq. (6)], and (f) orographic term [Eq. (4)] for the NCEP–NCAR 40-Year Reanalysis climatology. Contour intervals are 2 mm day^{-1}, and shading indicates negative values.

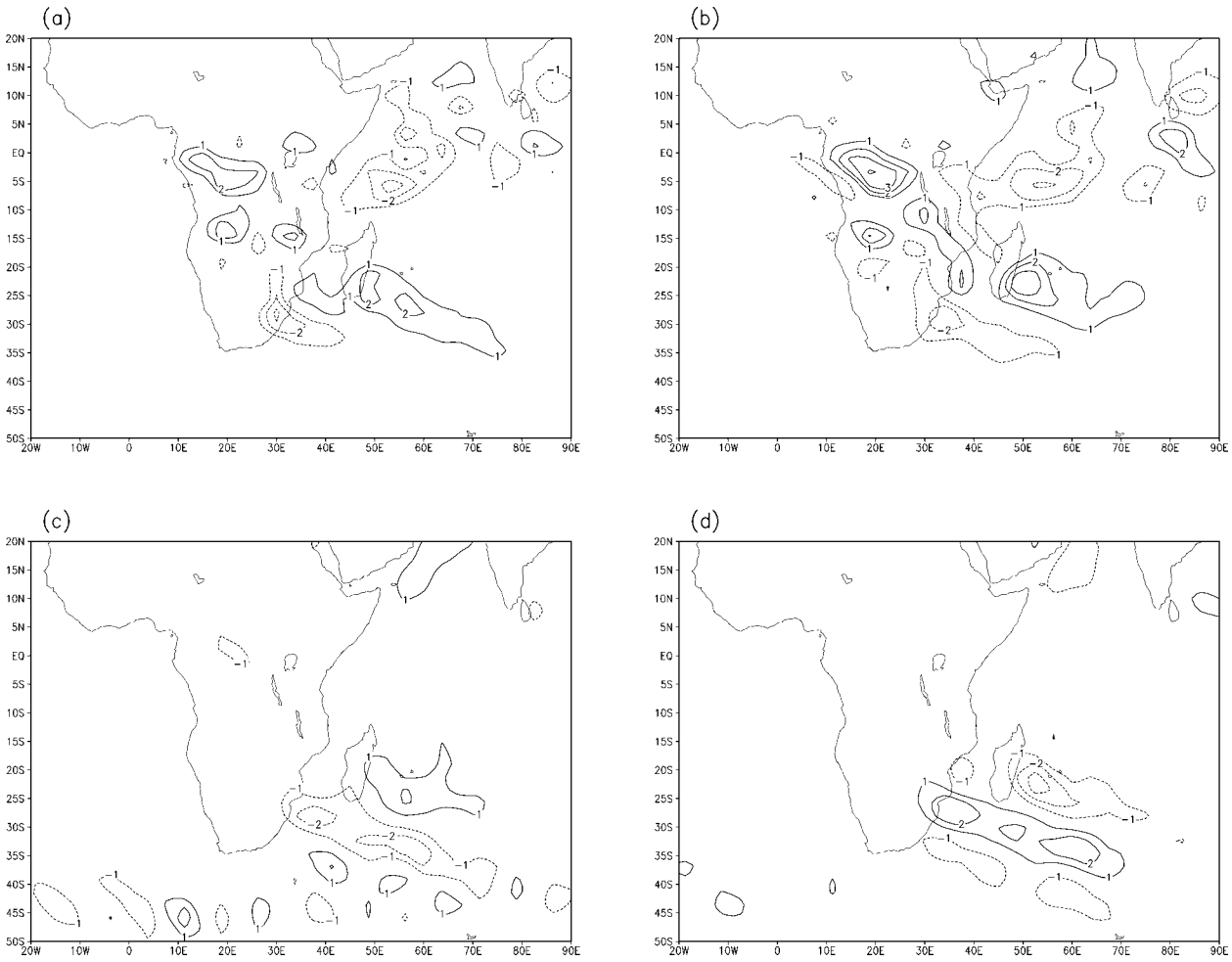

FIG. 9. (a) Precipitation anomaly due to ENSO SSTAs in the GCM ensemble simulation. Differences in components of the column moisture budget due to ENSO SSTAs in the GCM: (b) moisture convergence term, (c) moisture advection term, and (d) transients term. Contour intervals are 1 mm day^{-1} in each panel, and negative values are indicated by dashed contours.

in SST anomaly. Twenty 15-month ENSO integrations were conducted. Each integration has the same boundary conditions, including the time-dependent SST anomaly, but different initial conditions. The initial conditions for the 20 cases are instantaneous atmospheric states from a perpetual January integration of the model with the control (non-ENSO) boundary conditions. The ensemble members are averaged to form an ENSO climatology. The significance of the response to ENSO is measured against the ''natural'' variability of the control integration using a Student's *t* test for all variables except for precipitation. Since precipitation is poorly represented by the Gaussian probability distribution inherent in the Student's *t* test, the Wilcoxon–Mann–Whitney rank-sum test is used.

The broad response of the model is discussed in C00. Two waves are identified in the Southern Hemisphere subtropics and middle latitudes—one in the eastern hemisphere and one in the western. These are the only statistically significant wave responses. [The Pacific–North American (PNA) pattern occurs during December–February (DJF) in most, but not all, of the ensemble members, but it is not statistically significant even with 20 identical ENSO events and a 20-yr control integration.] As discussed by C00, these waves are generated in response to eastern Pacific warming. Here, the focus is the response of the southern African precipitation field to the eastern hemisphere wave.

Figure 9a shows the modeled precipitation perturbation over and near Africa in December due to ENSO. As discussed by C00, only precipitation perturbations in the central and eastern Pacific, in the SACZ, and in the SICZ were significant above the 90% level. The negative precipitation anomaly centered on the southeast coast near 30°S and 30°E and the positive anomaly to the northeast of this position are significant at the 99% confidence level. None of the other precipitation differences shown in Fig. 9a are statistically significant.

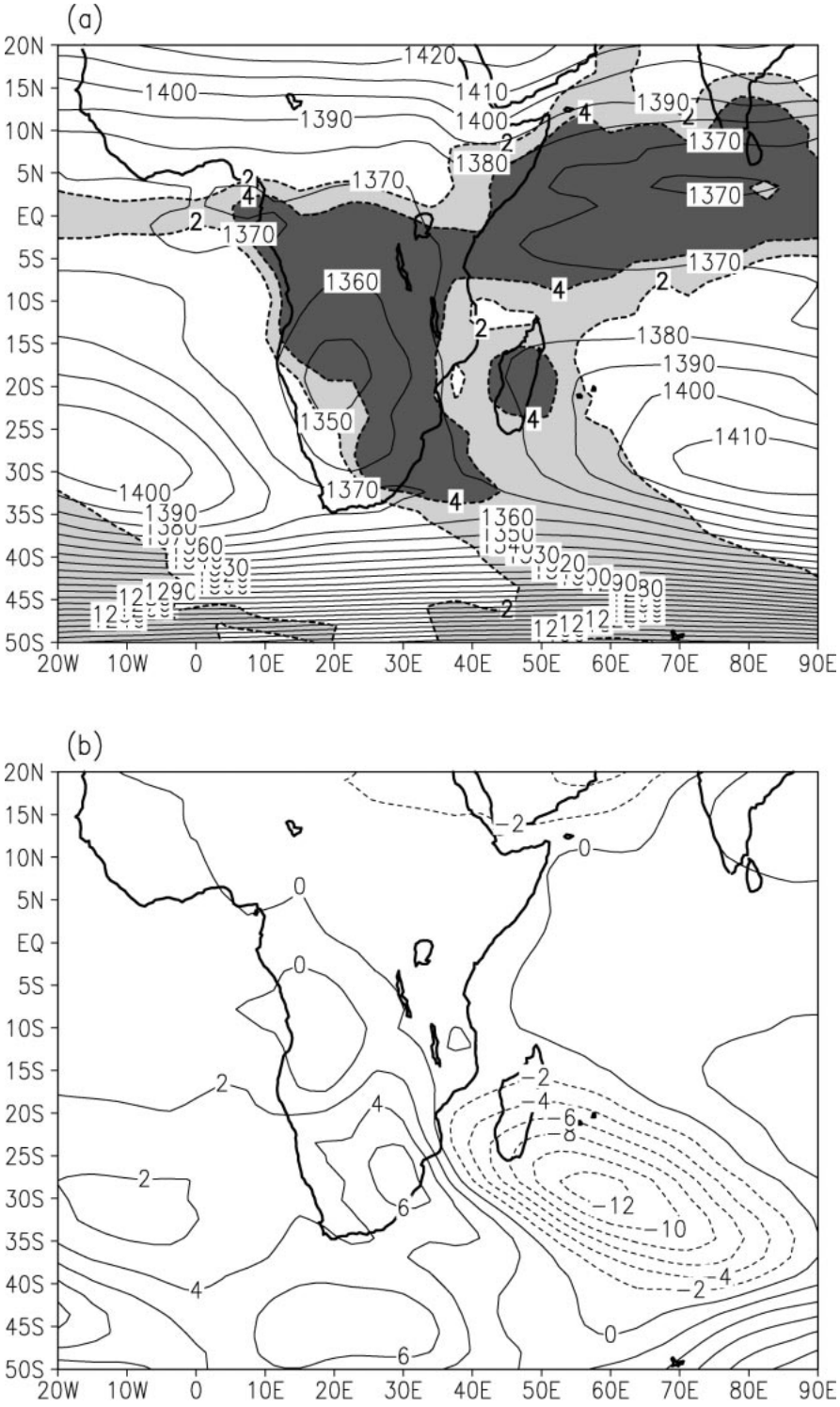

FIG. 10. (a) 866-mb geopotential heights from the GCM control climatology, using 10-gpm contour intervals. Precipitation rates are indicated by shading, with rates between 2 and 4 mm day^{-1} lightly shaded and rates greater than 4 mm day^{-1} more heavily shaded. (b) Contours of 866-mb geopotential height anomalies due to ENSO SSTAs in the GCM. Contour interval is 2 gpm.

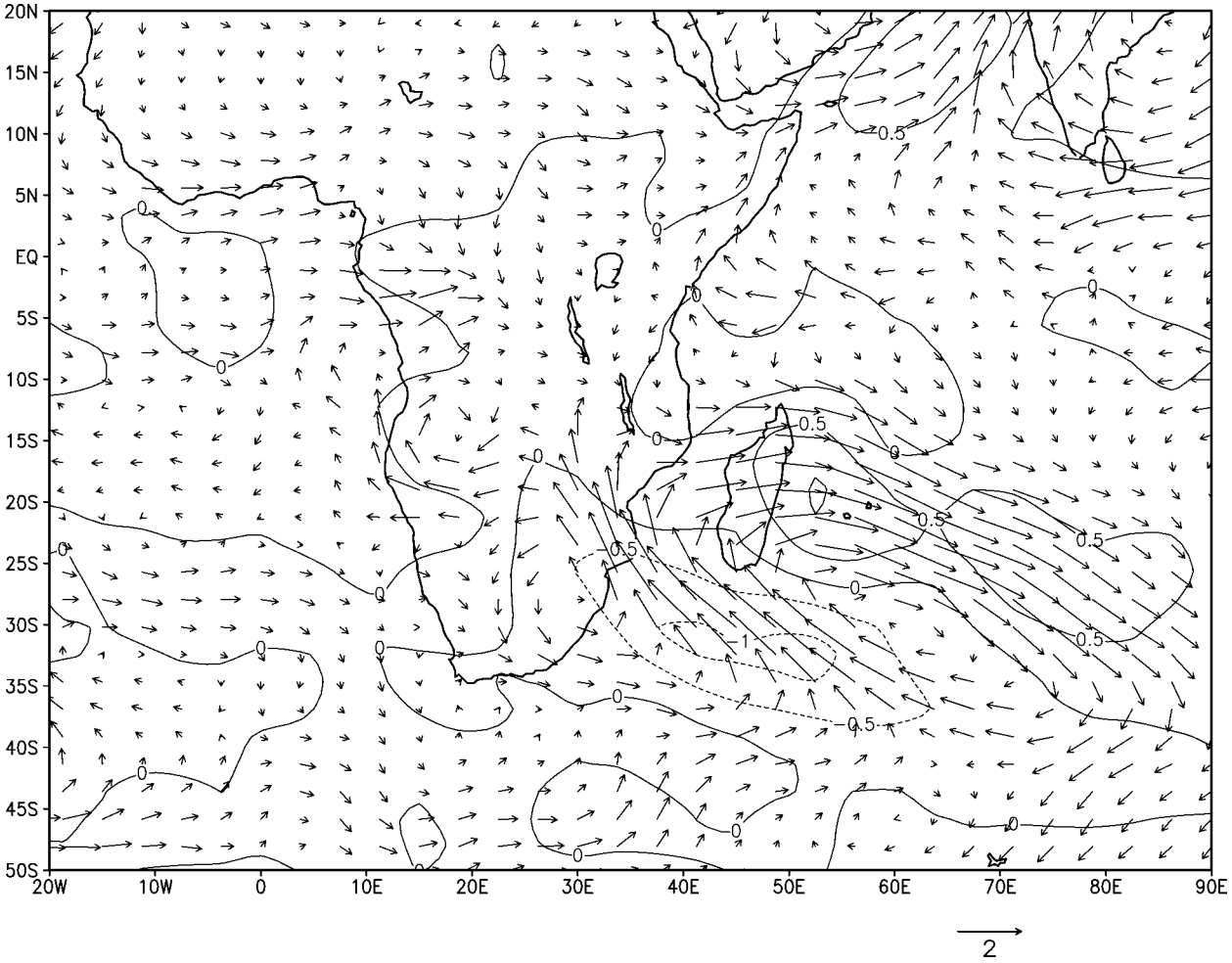

FIG. 11. Differences in the 866 mb water vapor mixing ratio and winds between the ENSO and control GCM climatologies. Contour interval is 0.5 g-H_2O kg^{-1} (vector scale: m s^{-1}).

The pattern is similar to the dipole precipitation anomalies that have been associated with ENSO as well as with other timescales of variability, as discussed in section 2.

The precipitation anomaly pattern over southeastern Africa and extending over the Indian Ocean suggests a northeastward shift of the SICZ. Such a shift results in higher precipitation over coastal Africa and Madagascar near 15°N and lower than normal precipitation to the southwest. This is consistent with the analysis of Shinoda and Kawamura (1996), who describe a circulation anomaly that is ''favorable to the simultaneous occurrence of a northward retraction . . . of the rainbelt'' over southeastern Africa in association with an ENSO-related empirical orthogonal function (EOF) mode in observed SSTs.

Other terms in the moisture budget are presented in Fig. 9. The moisture convergence (Fig. 9b), moisture advection (Fig. 9c), and transients (Fig. 9d) terms all contribute to the change in precipitation in the SICZ; evaporation and the orographic term do not. The convergence and advection terms both contribute to the northeastward shift of the SICZ, and transients oppose the shift.

Figure 10a shows 866-mb geopotential height contours from the control integration of the GCM. Similar to the idealized continent case and the reanalysis, the thermal low over the continent is deepest near the subsolar latitude, and the oceanic subtropical highs are centered 8°–10° latitude farther poleward. A midlatitude standing wave forms a trough off the southern coast, and it is about 15° east of its position in the reanalysis; it approximates the longitude of the boundary between the thermal low and the subtropical high. Shading in Fig. 10a indicates precipitation rates greater than 2 mm day^{-1} (light shading) and 4 mm day^{-1} (darker shading). The highest precipitation rates are associated with the equatorial trough, Madagascar, and the SICZ, which extends off the continent along the boundary between the thermal low and the subtropical high, as in the idealized continent simulation.

Figure 10b shows the 866-mb geopotential height

anomalies associated with the idealized ENSO events. Geopotential heights are lower by up to 12 gpm off the southeastern coast of Africa in the ENSO ensemble average. The anomaly represents a strengthening and eastward shift of the midlatitude trough, which Tyson (1986) and others have associated with dry spells over southeastern Africa. The positive height anomalies over the land surface are also expected during dry times and are consistent with observed anomalies (e.g., Matarira 1990).

The ENSO-induced geopotential perturbations coincide roughly with the precipitation perturbations (Fig. 9a) and could be interpreted as purely an effect of the shift in the precipitation field. For example, a positive precipitation anomaly would be associated with enhanced midtropospheric diabatic heating and, in the Tropics, increased upward vertical velocity and low heights below the heating maximum. Above the positive diabatic heating anomaly, higher heights would be expected. However, this is not the vertical structure that occurs. The negative anomalies shown in Fig. 10b persist to the tropopause, with magnitudes exceeding 50 gpm at 171 mb (see C00). Such barotropic vertical structure would not occur if the negative anomaly at low levels were being forced by midtropospheric heating anomalies.

As C00 shows, modifications in the vorticity transient forcing due to the idealized ENSO SSTAs are associated with a stationary wave in the eastern hemisphere. The geopotential perturbation shown in Fig. 10b is the first low in this wave. Because of the barotropic structure, the western portion of the subtropical high in the Indian Ocean is weakened throughout the depth of the troposphere. The SICZ is repositioned, and the precipitation maximum shifts to the northeast (Fig. 9a).

The anomalous flow within the SICZ is geostrophic to first order. Figure 11 shows anomalous 866-mb flow vectors and anomalous mixing ratio contours. The northeastward shift in the moisture advection term (Fig. 9c) is associated with the cyclonic circulation anomaly and also with the structure of the atmospheric moisture perturbation. Enhanced moisture advection occurs farther north because stronger winds blow off the continent and across the Mozambique Channel to Madagascar. East of Madagascar, the enhanced flow is also down the moisture gradient, and this supports the eastward extension of the SICZ in its shifted position (Fig. 9c). To the south–southeast, anomalous onshore easterly flow advects drier (midlatitude) air onto the continent. Lindesay et al. (1986) note a similar equatorward shift of the midlatitude westerlies during dry periods.

Column moisture convergence by transients (Fig. 9d) increases in the same location as the decreased moisture advection. We interpret this as an equatorward penetration of midlatitude air just east of South Africa, accompanied by enhanced storm activity.

6. Conclusions

Satellite-derived precipitation, an idealized GCM simulation, a realistic GCM simulation, and the NCEP–NCAR 40-Year Reanalysis are examined to argue for the existence of the South Indian convergence zone (SICZ). The SICZ is a land-based convergence zone (LBCZ) analogous to the South Atlantic convergence zone (SACZ). The SICZ is even more distinct than the SACZ in certain years, but it is less well defined in the mean climate. It is useful to interpret the observed precipitation in terms of an LBCZ instead of as a poleward excursion of the ITCZ in order to develop a physical understanding of certain aspects of precipitation variability over southern Africa.

The idealized GCM simulation is used to investigate the basic dynamics of an LBCZ. Simplified boundary conditions are prescribed in the model, with only one large, featureless continent included in a solstitial basic state. In the summer hemisphere, a diagonal band of enhanced precipitation stretches poleward and eastward off the continent between 10° and 40° latitude, extending 60° longitude to the east. In contrast to the ITCZ, where column moisture convergence is due to meridional wind convergence in the moist environment, the LBCZ is also supported by zonal wind convergence, moisture convergence by transient eddy activity, and moisture convergence associated with moisture advection. Zonal wind convergence between the flow in the subtropical high to the east of the continent and the thermal low supports a root zone for the LBCZ over the land surface. Extension out over the ocean is primarily due to the partially compensating influences of moisture advection and moist transient eddy activity, with meridional wind convergence also contributing.

The SICZ is prominent in the realistic GCM precipitation climatology but, as in the satellite-observed precipitation climatology, it does not clearly separate from the ITCZ in the NCEP–NCAR 40-Year Reanalysis climatology. The column moisture budgets in both the realistic GCM simulation and the reanalysis generally reproduce the distinctions between the moisture budgets of the ITCZ and the SICZ identified in the idealized model analysis. The most significant difference between the realistic cases and the idealized case is the interruption of strong zonal moisture convergence over the eastern regions of the continent. In the reanalysis, the SICZ is not well formed, mainly because moisture convergence by transient eddies more closely compensates for the moisture that occurs in association with advection off the continent. This suggests that interactions between transient and stationary eddy features and between tropical and midlatitude disturbances may be key to understanding how and why the SICZ moves, leading to the observed dipole pattern in precipitation, and why the SICZ is prominent in some years but not others.

In a GCM ensemble simulation of the response to warm ENSO SSTAs in the eastern Pacific, the SICZ

shifts northeastward because of a weakening of the South Indian subtropical high which, in turn, is related to a wave response forced indirectly from the eastern Pacific (C99). The resulting precipitation decrease over southern Africa in the model is similar to the observed precipitation reductions that often accompany warm events. Thus, a consideration of the SICZ and its dynamics leads to a physical understanding of the precipitation response.

The model results suggest that drying over southern Africa can occur purely as a consequence of the atmosphere's response to ENSO warming in the eastern Pacific. This is contrary to the results of Nicholson and Kim (1997), whose observational analysis suggests that the response over southern Africa is forced by SSTAs in the Atlantic and Indian Oceans. Most likely, the ENSO signal propagates into the southern African precipitation field from more than one source, adding to the difficulty in seasonal prediction.

Acknowledgments. This research was supported by award ATM-9815419 from NSF's Climate Dynamics Division. Thanks to B. Belcher, T. Duffy, and E. Vizy for useful comments on an earlier version of this paper and to B. Belcher for also helping to prepare the figures. Thanks also to an anonymous reviewer whose suggestions resulted in an improved paper.

REFERENCES

Arkin, P. A., and B. N. Meisner, 1987: The relationship between large-scale convective rainfall and cold cloud cover over the Western Hemisphere during 1982–1984. *Mon. Wea. Rev.,* **115,** 51–74.

Cook, K. H., 1994: Mechanisms by which surface drying perturbs tropical precipitation fields. *J. Climate,* **7,** 400–413.

——, 1997: Large-scale atmospheric dynamics and Sahelian precipitation. *J. Climate,* **10,** 1137–1152.

——, 1998: On the response of the Southern Hemisphere to ENSO. *Proc. 23rd Climate Diagnostics and Prediction Workshop,* Miami, FL, Amer. Meteor. Soc., 323–326.

Janowiak, J. J., 1988: An investigation of interannual rainfall variability in Africa. *J. Climate,* **1,** 240–255.

Jury, M. R., 1992: A climatic dipole governing the interannual variability of convection over the SW Indian Ocean and SE Africa region. *Trends Geophys. Res.,* **1,** 165–172.

——, C. McQueen, and K. Levey, 1994: SOI and QBO signals in the African region. *Theor. Appl. Climatol.,* **50,** 103–115.

Kalnay, E., and Coauthors, 1996: The NCEP/NCAR 40-Year Reanalysis Project. *Bull. Amer. Meteor. Soc.,* **77,** 437–471.

Kuhnel, I., 1989: Tropical–extratropical cloud band climatology based on satellite data. *Int. J. Climatol.,* **9,** 441–463.

Latif, M., and T. P. Barnett, 1995: Interactions of the tropical oceans. *J. Climate,* **8,** 952–964.

Lenters, J. D., and K. H. Cook, 1995: Simulation and diagnosis of the regional South American precipitation climatology. *J. Climate,* **8,** 2988–3005.

——, and ——, 1999: Summertime precipitation variability in South America: Role of the large-scale circulation. *Mon. Wea. Rev.,* **127,** 409–431.

Lindesay, J. A., 1988: South African rainfall, the Southern Oscillation and a Southern Hemisphere semi-annual cycle. *J. Climatol.,* **8,** 17–30.

——, M. S. J. Harrison, and M. P. Haffner, 1986: The Southern Oscillation and South African rainfall. *South Afr. J. Sci.,* **82,** 196–198.

Lyons, S. W., 1991: Origins of convective variability over equatorial southern Africa during austral summer. *J. Climate,* **4,** 23–39.

Mason, S. J., 1995: Sea surface temperature–South African rainfall associations, 1910–1989. *Int. J. Climatol.,* **15,** 119–135.

——, and M. R. Jury, 1997: Climatic variability and change over southern Africa: A reflection on underlying processes. *Prog. Phys. Geogr.,* **21,** 23–50.

Matarira, C. H., 1990: Drought over Zimbabwe in a regional and global context. *Int. J. Climatol.,* **10,** 609–625.

Matthews, E., 1983: Global vegetation and land use: New high-resolution data bases for climate studies. *J. Climate Appl. Meteor.,* **22,** 474–487.

Mintz, Y., and G. K. Walker, 1993: Global fields of moisture and land surface evapotranspiration derived from observed precipitation and surface air temperature. *J. Appl. Meteor.,* **32,** 1305–1334.

Nicholson, S. E., and D. Entekhabi, 1987: Rainfall variability in equatorial and southern Africa: Relationships with sea surface temperatures along the southwestern coast of Africa. *J. Climate Appl. Meteor.,* **26,** 561–578.

——, and J. Kim, 1997: The relationship of the El Niño–Southern Oscillation to African rainfall. *Int. J. Climatol.,* **17,** 117–135.

Paegle, J., and K. Mo, 1997: Alternating wet and dry conditions over South America in summer. *Mon. Wea. Rev.,* **125,** 279–291.

Ringler, T. D., and K. H. Cook, 1995: Orographically-induced stationary waves: Dependence on latitude. *J. Atmos. Sci.,* **52,** 2548–2560.

Ropelewski, C. F., and M. S. Halpert, 1987: Global and regional scale precipitation patterns associated with the El Niño/Southern Oscillation. *Mon. Wea. Rev.,* **115,** 1606–1626.

Shannon, L. V., J. R. E. Lutjeharms, and G. Nelson, 1990: Causative mechanisms for intra-annual and interannual variability in the marine environment around southern Africa. *South Afr. J. Sci.,* **86,** 356–373.

Shea, D. J., K. E. Trenberth, and R. W. Reynolds, 1992: A global monthly sea surface temperature climatology. *J. Climate,* **5,** 987–1001.

Shinoda, M., and R. Kawamura, 1996: Relationships between rainfall over semi-arid southern Africa, geopotential heights, and sea surface temperatures. *J. Meteor. Soc. Japan,* **74,** 21–36.

Stoeckenius, T., 1981: Interannual variations of tropical precipitation patterns. *Mon. Wea. Rev.,* **109,** 1233–1247.

Streten, N. A., 1973: Some characteristics of satellite-observed bands of persistent cloudiness over the Southern Hemisphere. *Mon. Wea Rev.,* **101,** 486–495.

Taljaard, J. J., 1953: The mean circulation in the lower troposphere over southern Africa. *South Afr. Geogr. J.,* **35,** 33–45.

Todd, M., and R. Washington, 1998: Extreme daily rainfall in southern Africa and southwest Indian Ocean: Tropical–temperate links. *South Afr. J. Sci.,* **94,** 64–70.

Tyson, P. D., 1986: *Climatic Change and Variability in Southern Africa.* Oxford University Press, 220 pp.

Walker, N. D., and F. A. Shillington, 1990: The effect of oceanographic variability on South African weather and climate. *South Afr. J. Sci.,* **86,** 382–386.